Available online at www.sciencedirect.com
ScienceDirect
Journal of Sound and Vibration 323 (2009) 737–756
JOURNAL OF SOUND AND VIBRATION
www.elsevier.com/locate/jsvi

Free and forced vibrations of a tyre using a wave/finite element approach

Y. Waki*, B.R. Mace, M.J. Brennan

Institute of Sound and Vibration Research, University of Southampton, Highfield, Southampton SO17 1BJ, UK

Received 22 July 2008; received in revised form 19 December 2008; accepted 8 January 2009
Handling Editor: C.L. Morfey
Available online 8 February 2009

Abstract

Free and forced vibrations of a tyre are predicted using a wave/finite element (WFE) approach. A short circumferential segment of the tyre is modelled using conventional finite element (FE) methods, a periodicity condition applied and the mass and stiffness matrices post-processed to yield wave properties. Since conventional FE methods are used, commercial FE packages and existing element libraries can be utilised. An eigenvalue problem is formulated in terms of the transfer matrix of the segment. Zhong's method is used to improve numerical conditioning. The eigenvalues and eigenvectors give the wavenumbers and wave mode shapes, which in turn define transformations between the physical and wave domains. A method is described by which the frequency dependent material properties of the rubber components of the tyre can be included without the need to remesh the structure. Expressions for the forced response are developed which are numerically well-conditioned. Numerical results for a smooth tyre are presented. Dispersion curves for real, imaginary and complex wavenumbers are shown. The propagating waves are associated with various forms of motion of the tread supported by the stiffness of the side wall. Various dispersion phenomena are observed, including curve veering, non-zero cut-off and waves for which the phase velocity and the group velocity have opposite signs. Results for the forced response are compared with experimental measurements and good agreement is seen. The forced response is numerically determined for both finite area and point excitations. It is seen that the size of area of the excitation is particularly important at high frequencies. When the size of the excitation area is small enough compared to the tread thickness, the response at high frequencies becomes stiffness-like (reactive) and the effect of shear stiffness becomes important.

1. Introduction

Tyre noise is a significant source of traffic noise at speeds over 40 km/h for passenger cars and over 60 km/h for heavy lorries [1]. Understanding the vibrational behaviour of a tyre is thus becoming more important. Measured spectra of tyre noise show a broad peak around 1 kHz at which frequency the wavelengths in the tyre are short. At such high frequencies the computational cost of full finite element analysis (FEA) becomes impractically large, e.g. [2,3]. Alternative approaches are therefore of interest and especially those based on the response of the tyre in terms of waves.

*Corresponding author. Tel.: +44 23 8059 4175; fax: +44 23 8059 3190.
E-mail address: waki.yoshiyuki@bridgestone.co.jp (Y. Waki).

0022-460X/$ - see front matter © 2009 Elsevier Ltd. All rights reserved.
doi:10.1016/j.jsv.2009.01.006

For simple structures such as a thin rod or a thin beam, wave properties (propagation, response for external excitation, transmission and reflection) can be obtained analytically from the equations of motion, e.g. [4]. Several simple analytical wave models have been proposed to investigate waves in a tyre. The classical and simple one-dimensional model using a curved beam subjected to in-plane tension and lying on an elastic foundation was proposed by Böhm [5]. Pinnington extended the one-dimensional model to include the shear stiffness and the rotary inertia of the tread and considered both shear and rotational waves [6]. Two-dimensional models have been proposed by several researchers. Kropp et al. [7,8] developed a model for a layered flat plate on an elastic foundation. They also investigated the contact model and the noise radiation from a tyre [9]. Their extensive work is summarised in Refs. [10,11]. Pinnington modelled a tyre as a beam and a plate on a sidewall impedance [12,13]. Muggleton et al. [14] modelled a tyre as three flat plates jointed by springs. However, it is difficult or impossible to include details of practical tyre constructions in these analytical models, hence other numerical solutions are desired.

A tyre is a complicated structure composed of steel and textile fibre-reinforced rubber sheets and several different rubbers. A typical cross-section of a commercial tyre is illustrated in Fig. 1. Relatively few works have investigated waves in a tyre using numerical methods. Bolton et al. [15,16] estimated the dispersion curves from experimental data and from an FE model of a cylinder representing a tyre, but this approach provides only approximate estimates of the propagating wavenumbers from measured or predicted natural frequencies. An alternative numerical approach to investigate waves in complicated structures is the spectral finite element (SFE) method, e.g. [17–20]. In the SFE method, the equation of motion is projected into the wave domain such that

$$\left[\sum_i (-\mathrm{j}k)^i \bar{\mathbf{K}}_i - \omega^2 \bar{\mathbf{M}}\right]\mathbf{q} = \mathbf{f} \tag{1}$$

where k is the wavenumber, $\bar{\mathbf{K}}$ and $\bar{\mathbf{M}}$ are the spectral stiffness and mass matrices, $\mathbf{q}$ is the vector of nodal degrees of freedom (DOFs), $\mathbf{f}$ is the forcing vector, $\mathrm{j} = \sqrt{-1}$ and i is an integer. For real wavenumbers and stiffness matrices, the solutions to Eq. (1) for real ω may be found by solving a standard linear eigenvalue problem. However, the wavenumber k may be complex such that solutions of k must be found for given real ω. In this case the eigenvalue problem becomes polynomial which is less easy to solve and more prone to numerical conditioning problems. Nilsson [19] considered the application of the SFE method to a tyre. He assumed the tyre to be a thin structure and modelled it using spectral shell elements. However, the method needs special elements to be developed on demand which is not an insignificant task.

An alternative approach, the wave/finite element (WFE) method [21,22], can be used to investigate the dynamic properties of complicated waveguides and is applied in this paper to the analysis of a realistic automotive tyre. The method starts from an FE model of only a short segment of the waveguide. Since conventional FE methods can be used for modelling the cross-section of the waveguide, existing commercial FE packages, their meshing capabilities and element libraries can be fully utilised. The method involves forming the mass and stiffness matrices of the segment of the waveguide, applying a periodicity condition and post-processing the results to form an eigenvalue problem, whose solution yields the wavenumbers and wave

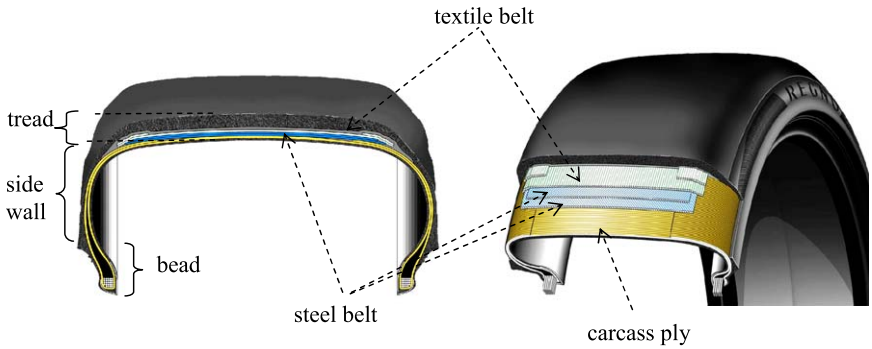

Fig. 1. Cross-section of a tyre.

mode shapes. The approach adopted below is to formulate and solve a well-conditioned eigenvalue problem, found from the dynamic stiffness matrix of the segment. In the literature, the WFE method has been applied to investigate free wave propagation in a layered sandwich beam [21], a fluid-filled pipe [23] and thin-walled structures [24]. The forced response can be calculated using wave properties. In the literature Duhamel et al. [22] presented a formulation for calculating the forced response. Thompson [25] calculated the forced response based on the receptance approach for a railway track. However, these approaches potentially suffer from ill-conditioning problems for general waveguides for which the cross-section has many DOFs and care needs to be taken to reduce these.

This paper describes free wave propagation and the forced response of a tyre using the WFE method. Frequency dependent material properties of rubber [26] are included in the stiffness matrix without the need to remodel the structure. If the structure is damped the wavenumbers become complex and are associated with spatially decaying waves. In such a case the WFE method is particularly useful. By using numerically determined freely propagating and decaying waves, a wave approach is developed to calculate the forced response. A well-conditioned formulation for numerically determining the amplitudes of the directly excited waves is found by exploiting the orthogonality of the left and right eigenvectors. Wave amplitudes at a location in the tyre are calculated by considering wave propagation and the response is then determined by superimposing the wave amplitudes at the response point. The predicted forced response is compared with experiment and good agreement is seen.

In the next section the WFE method is briefly reviewed. Section 3 concerns determination of the forced response of a waveguide. In Section 4 the WFE method is applied to a tyre with frequency dependent elastic properties. Sections 5 and 6 contain simulations and experimental results.

2. Formulation of the WFE method

The method by which wave properties are extracted from an FE model of a short segment of a waveguide is described in this section. Further details can be found for example in Refs. [21,27]. The WFE method starts from an FE model of only a short segment of the waveguide. The dynamic stiffness matrix of the segment is obtained and a periodicity condition applied. This results in an eigenvalue problem which can be formulated in a number of ways. The eigenvalue problem is prone to poor numerical conditioning, especially for one-dimensional waveguides, such as the tyre, for which there are many dofs across the cross-section. For such cases, and especially when damping is present, care needs to be taken in the formulation of the eigenvalue problem. The approaches, together with issues concerning numerical conditioning, are described.

2.1. Dynamic stiffness matrix

Consider a short of segment of length Δ of a uniform waveguide as shown in Fig. 2. The equation for time harmonic motion of the segment can be written as

$$\mathbf{Dq} = \mathbf{f} \tag{2}$$

where

$$\mathbf{D} = \mathbf{K} + \mathrm{j}\omega\mathbf{C} - \omega^2\mathbf{M} \tag{3}$$

is the dynamic stiffness matrix, $\mathbf{q}$ and $\mathbf{f}$ the vectors of nodal dofs and forces and $\mathbf{K}$, $\mathbf{C}$ and $\mathbf{M}$ are the stiffness, viscous damping and mass matrices which are formed using conventional FE methods. The stiffness matrix $\mathbf{K}$ may be complex if structural damping is present. Time harmonic motion $\exp(\mathrm{j}\omega t)$ is implicit throughout this

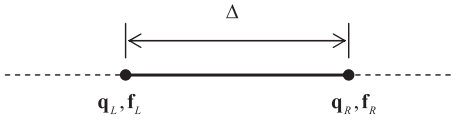

Fig. 2. A segment of a uniform waveguide.

paper. Eq. (3) can be rearranged in matrix form as

$$\begin{bmatrix} \mathbf{D}_{LL} & \mathbf{D}_{LR} \\ \mathbf{D}_{RL} & \mathbf{D}_{RR} \end{bmatrix} \begin{bmatrix} \mathbf{q}_L \\ \mathbf{q}_R \end{bmatrix} = \begin{bmatrix} \mathbf{f}_L \\ \mathbf{f}_R \end{bmatrix} \tag{4}$$

where the subscripts L and R represent the left and right hand sides of the segment. For uniform waveguides

$$\mathbf{D}_{LL}^{\mathrm{T}} = \mathbf{D}_{LL}, \quad \mathbf{D}_{RR}^{\mathrm{T}} = \mathbf{D}_{RR}, \quad \mathbf{D}_{LR}^{\mathrm{T}} = \mathbf{D}_{RL} \tag{5}$$

where $(\cdot)^{\mathrm{T}}$ indicates the transpose.

If the section has internal nodes as shown in Fig. 3, the associated dofs can be condensed. When no external force is applied to the internal nodes the equation of motion may be expressed as

$$\begin{bmatrix} \tilde{\mathbf{D}}_{LL} & \tilde{\mathbf{D}}_{LR} & \tilde{\mathbf{D}}_{LI} \\ \tilde{\mathbf{D}}_{RL} & \tilde{\mathbf{D}}_{RR} & \tilde{\mathbf{D}}_{RI} \\ \tilde{\mathbf{D}}_{IL} & \tilde{\mathbf{D}}_{IR} & \tilde{\mathbf{D}}_{II} \end{bmatrix} \begin{bmatrix} \mathbf{q}_L \\ \mathbf{q}_R \\ \mathbf{q}_I \end{bmatrix} = \begin{bmatrix} \mathbf{f}_L \\ \mathbf{f}_R \\ \mathbf{0} \end{bmatrix} \tag{6}$$

The subscript I represents dofs which are associated with the internal nodes. These can be dynamically condensed as [27,28]

$$[\tilde{\mathbf{D}}_{MM} - \tilde{\mathbf{D}}_{MI}\tilde{\mathbf{D}}_{II}^{-1}\tilde{\mathbf{D}}_{IM}]\mathbf{q}_M = \mathbf{f}_M \tag{7}$$

where

$$\tilde{\mathbf{D}}_{MM} = \begin{bmatrix} \tilde{\mathbf{D}}_{LL} & \tilde{\mathbf{D}}_{LR} \\ \tilde{\mathbf{D}}_{RL} & \tilde{\mathbf{D}}_{RR} \end{bmatrix}, \quad \tilde{\mathbf{D}}_{MI} = \begin{bmatrix} \tilde{\mathbf{D}}_{LI} \\ \tilde{\mathbf{D}}_{RI} \end{bmatrix}, \quad \tilde{\mathbf{D}}_{IM} = [\tilde{\mathbf{D}}_{IL} \;\; \tilde{\mathbf{D}}_{IR}], \quad \mathbf{q}_M = \begin{bmatrix} \mathbf{q}_L \\ \mathbf{q}_R \end{bmatrix}, \quad \mathbf{f}_M = \begin{bmatrix} \mathbf{f}_L \\ \mathbf{f}_R \end{bmatrix} \tag{8}$$

In this paper any dofs associated with internal nodes are condensed so that the resulting equation of motion has the form of Eq. (4).

2.2. Transfer matrix and transformation to the wave domain

Under the passage of a wave with wavenumber k, a periodicity condition [29] holds so that

$$\mathbf{q}_R = \lambda \mathbf{q}_L; \quad \lambda = \exp(-\mathrm{j}k\Delta) \tag{9}$$

while equilibrium implies that

$$[\lambda\mathbf{I} \;\; \mathbf{I}]\begin{Bmatrix} \mathbf{f}_L \\ \mathbf{f}_R \end{Bmatrix} = \mathbf{0} \tag{10}$$

and $\mathbf{I}$ is the identity matrix. These equations can be used to project Eq. (4) onto the dofs $\mathbf{q}_L$ by premultiplying by $[\lambda\mathbf{I} \;\; \mathbf{I}]$. This results in an eigenvalue problem which, in principle, yields the eigenvalues λ and consequent eigenvectors (the wave mode shapes) but this formulation is prone to poor numerical conditioning and an approach based on Zhong's method [30], described later in this section, is preferred.

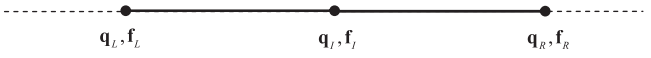

Fig. 3. A segment with an internal node.

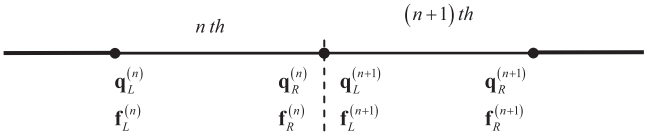

Fig. 4. A series of segments.

Consider a series of segments of the waveguide as shown in Fig. 4. Continuity of displacement and force equilibrium of adjacent segments then gives

$$\begin{bmatrix} \mathbf{q}_L^{(n+1)} \\ \mathbf{f}_L^{(n+1)} \end{bmatrix} = \begin{bmatrix} \mathbf{q}_R^{(n)} \\ -\mathbf{f}_R^{(n)} \end{bmatrix} = \mathbf{T} \begin{bmatrix} \mathbf{q}_L^{(n)} \\ \mathbf{f}_L^{(n)} \end{bmatrix} = \lambda \begin{bmatrix} \mathbf{q}_L^{(n)} \\ \mathbf{f}_L^{(n)} \end{bmatrix} \tag{11}$$

where $\mathbf{T}$ is the transfer matrix. Free wave motion over any section of length Δ is therefore described in the form of an eigenvalue problem such that

$$\mathbf{T}\boldsymbol{\phi}_i = \lambda_i \boldsymbol{\phi}_i. \tag{12}$$

The transfer matrix $\mathbf{T}$ is given in terms of the elements of the dynamic stiffness matrix by [21,22]

$$\mathbf{T} = \begin{bmatrix} -\mathbf{D}_{LR}^{-1}\mathbf{D}_{LL} & \mathbf{D}_{LR}^{-1} \\ -\mathbf{D}_{RL} + \mathbf{D}_{RR}\mathbf{D}_{LR}^{-1}\mathbf{D}_{LL} & -\mathbf{D}_{RR}\mathbf{D}_{LR}^{-1} \end{bmatrix}. \tag{13}$$

The eigenvalue λ_i in Eq. (12) describes wave propagation over a distance Δ such that [29]

$$\lambda_i = \exp(-\mathrm{j}k_i\Delta) \tag{14}$$

where k_i represents the wavenumber for the ith wave as in Eq. (9). The wavenumber can be purely real, purely imaginary or complex, associated with a propagating, a nearfield (evanescent) or an oscillating decaying wave, respectively. The right eigenvector corresponding to the ith eigenvalue can be written as

$$\boldsymbol{\phi}_i = \begin{Bmatrix} \boldsymbol{\phi}_{q,i} \\ \boldsymbol{\phi}_{f,i} \end{Bmatrix} \tag{15}$$

The eigenvector represents a wave mode and describes the nodal displacements $\boldsymbol{\phi}_{q,i}$ and associated internal forces $\boldsymbol{\phi}_{f,i}$ under the passage of the ith wave.

The eigenvalues come in pairs and are of the form $\lambda_i^{\pm} = \exp(\pm\mathrm{j}k_i\Delta)$, which represent positive- and negative-going wave pairs. The eigenvalues and associated eigenvectors are then expressed as $(\lambda_i, \boldsymbol{\phi}_i^+)$ and $(1/\lambda_i, \boldsymbol{\phi}_i^-)$. Positive-going waves are those for which $|\lambda_i| < 1$, i.e. the amplitude decreases in the direction of propagation, or if $|\lambda_i| = 1$, the power is positive, i.e. $\mathrm{Re}\{\mathrm{i}\omega\boldsymbol{\phi}_{f,i}^{\mathrm{H}}\boldsymbol{\phi}_{q,i}\} < 0$ [21,31] where $(\cdot)^{\mathrm{H}}$ represents the complex conjugate transpose, or Hermitian.

The eigenvalue problem (12) may be written using the eigenvalues and left eigenvectors as

$$\boldsymbol{\psi}_i\mathbf{T} = \lambda_i\boldsymbol{\psi}_i \tag{16}$$

The left and right eigenvalues are identical, while the orthogonality relations between the left and right eigenvectors can be expressed as

$$\boldsymbol{\psi}_i\boldsymbol{\phi}_j = d_i\delta_{ij} \tag{17}$$

where δ_{ij} is the Kronecker delta and d_i is arbitrary. It is often convenient to normalise the eigenvectors such that $d_i = 1$.

The matrices

$$\boldsymbol{\Phi}_q^+ = [\boldsymbol{\phi}_{q,1}^+ \;\; \boldsymbol{\phi}_{q,2}^+ \;\; \cdots \;\; \boldsymbol{\phi}_{q,n}^+]; \quad \boldsymbol{\Psi}_q^+ = \begin{Bmatrix} \boldsymbol{\psi}_{q,1}^+ \\ \boldsymbol{\psi}_{q,2}^+ \\ \\ \boldsymbol{\psi}_{q,n}^+ \end{Bmatrix} \tag{18}$$

can be formed from the eigenvectors, n being the total number of dofs on the left hand side of the modelled segment. Similar expressions hold for $\boldsymbol{\Phi}_q^-, \boldsymbol{\Psi}_q^-, \boldsymbol{\Phi}_f^{\pm}$ and $\boldsymbol{\Psi}_f^{\pm}$. These matrices, together with the orthogonality relations of Eq. (17), define transformations between the physical domain, in which the motion is described in terms of $\mathbf{q}$ and $\mathbf{f}$ and the wave domain, in which the motion is described in terms of the amplitudes $\mathbf{a}^+$ and $\mathbf{a}^-$

of the waves travelling in the positive and negative directions, respectively. Specifically

$$\mathbf{q} = \mathbf{\Phi}_q^+ \mathbf{a}^+ + \mathbf{\Phi}_q^- \mathbf{a}^-; \quad \mathbf{f} = \mathbf{\Phi}_f^+ \mathbf{a}^+ + \mathbf{\Phi}_f^- \mathbf{a}^-. \tag{19}$$

In practice, as in modal analysis, only a number m of the wave modes might be kept, so that the matrices $\mathbf{\Phi}_{q,f}^{\pm}$ and $\mathbf{\Psi}_{q,f}^{\pm}$ are $n \times m$ and $m \times n$, respectively. The kept (positive-going) wave modes would be those for which $|\lambda|$ is close to unity. The reasons for reducing the size of the wave basis are partly that the size of the model is smaller, but primarily that the calculation of the high order wave modes, which decay very rapidly with distance (by orders of magnitude over the element length), is prone to poor numerical conditioning.

2.3. Conditioning of the eigenvalue problem

The eigenvalue problem of Eq. (12) may suffer from poor numerical conditioning, typically because there are often both very large and very small eigenvalues. These represent wave modes that attenuate very rapidly with distance either in the positive or negative direction. Conditioning can be improved using Zhong's method [30], which exploits the symplectic properties of the system matrices. The method starts from a reformulation of Eq. (12) into the relationships for the displacement vectors alone. After some manipulation, the eigenvalue problem becomes

$$\begin{bmatrix} \mathbf{0} & \mathbf{D}_{LR} \\ -\mathbf{D}_{RL} & \mathbf{0} \end{bmatrix} \begin{bmatrix} \boldsymbol{\phi}_{q,i} \\ \lambda \boldsymbol{\phi}_{q,i} \end{bmatrix} = 1(\lambda_i + 1/\lambda_i) \begin{bmatrix} (\mathbf{D}_{LR} - \mathbf{D}_{RL}) & -(\mathbf{D}_{LL} + \mathbf{D}_{RR}) \\ (\mathbf{D}_{LL} + \mathbf{D}_{RR}) & (\mathbf{D}_{LR} - \mathbf{D}_{RL}) \end{bmatrix} \begin{bmatrix} \boldsymbol{\phi}_{q,i} \\ \lambda_i \boldsymbol{\phi}_{q,i} \end{bmatrix}. \tag{20}$$

Note that the eigenvalues of most interest are those for which $|\lambda + 1/\lambda|$ is the smallest. This eigenvalue problem has repeated eigenvalues of $\lambda + 1/\lambda$. The original displacement eigenvectors in Eq. (15) are given by a linear combination of the repeated eigenvectors of Eq. (20) [21,22]. The force eigenvectors are given from the first row of Eq. (4) together with Eq. (9) by

$$\boldsymbol{\phi}_{f,i} = (\mathbf{D}_{LL} + \lambda_i \mathbf{D}_{LR}) \boldsymbol{\phi}_{q,i}. \tag{21}$$

Numerical issues concerning the determination of the eigenvectors and an application of singular value decomposition to improve numerical difficulties are described in Refs. [27,32].

In this paper the formulation (20) is used to determine free wave propagation characteristics in a tyre.

2.4. Group velocity

The group velocity is the velocity at which the energy propagates. The group velocity $c_{g,i}$ for the ith wave mode can be calculated from power and energy as [21,33]

$$c_{g,i} = \frac{P_i}{E_{\mathrm{tot},i}} \tag{22}$$

where

$$P_i = -\frac{1}{2} \mathrm{Re}\{\mathrm{j}\omega \boldsymbol{\phi}_{f,i}^{\mathrm{H}} \boldsymbol{\phi}_{q,i}\} = -\frac{\omega}{2} \mathrm{Im}\{\boldsymbol{\phi}_{f,i}^{\mathrm{H}} \boldsymbol{\phi}_{q,i}\} \tag{23}$$

is the time-averaged power transmitted thorough the cross-section and E_{tot} is the total energy density per unit length. This is given by

$$\begin{aligned} E_{\mathrm{tot},i} &= E_{p,i} + E_{k,i}, \\ E_{p,i} &= \frac{1}{4\Delta} \mathrm{Re}\left\{ [\boldsymbol{\phi}_{q,i}^{\mathrm{H}} \;\; \lambda_i \boldsymbol{\phi}_{q,i}^{\mathrm{H}}] \mathbf{K} \begin{Bmatrix} \boldsymbol{\phi}_{q,i} \\ \lambda_i \boldsymbol{\phi}_{q,i} \end{Bmatrix} \right\}, \\ E_{k,i} &= -\frac{\omega^2}{4\Delta} \mathrm{Re}\left\{ [\boldsymbol{\phi}_{q,i}^{\mathrm{H}} \;\; \lambda_i \boldsymbol{\phi}_{q,i}^{\mathrm{H}}] \mathbf{M} \begin{Bmatrix} \boldsymbol{\phi}_{q,i} \\ \lambda_i \boldsymbol{\phi}_{q,i} \end{Bmatrix} \right\} \end{aligned} \tag{24}$$

where $E_{p,i}$ and $E_{k,i}$ represent the potential and kinetic energy densities for the ith wave mode. The dissipated power follows from the imaginary part of $\mathbf{K}$ and/or the damping matrix $\mathbf{C}$.

3. Forced response using a wave approach

The forced response of a waveguide can be calculated from knowledge of the properties of wave propagation. The steps involved are: (1) solving for free wave propagation; (2) determining the amplitudes of directly excited waves assuming the waveguide is infinite; (3) determining the reflection and transmission matrices for boundaries etc; (4) superimposing wave amplitudes at a response point by considering wave propagation between various stations in the waveguide. When a waveguide forms a ring, such as the tyre considered here, step (3) is not required, there being no boundaries. The formulation presented here is well-conditioned and can be used for general waveguides in which there are many wave modes.

3.1. Determining the amplitudes of directly excited waves

Eq. (19) provides a transformation by which the displacement and forces in the physical domain can be represented in the wave domain, e.g. [34]. To calculate the amplitudes of the directly excited waves, an external force in the physical domain is first decomposed into the wave domain. When an external excitation $\mathbf{f}_{\text{ext}}$ is applied to an infinite waveguide at a point as shown in Fig. 5, continuity of displacement and force equilibrium at the excitation point give in matrix form

$$\begin{bmatrix} \mathbf{\Phi}_q^+ & -\mathbf{\Phi}_q^- \\ \mathbf{\Phi}_f^+ & -\mathbf{\Phi}_f^- \end{bmatrix} \begin{bmatrix} \mathbf{e}^+ \\ \mathbf{e}^- \end{bmatrix} = \begin{bmatrix} \mathbf{0} \\ \mathbf{f}_{\text{ext}} \end{bmatrix} \tag{25}$$

where $\mathbf{e}^{\pm}$ are column vectors of the amplitudes of the directly excited waves and the matrices $\mathbf{\Phi}_q^{\pm}$, $\mathbf{\Phi}_f^{\pm}$ contain the kept displacement and force eigenvectors. As discussed in Section 2.2, the direction of wave propagation is determined by the magnitude of the wavenumber or the direction of energy flow for undamped waves, i.e. the sign of the group velocity. If all the wave modes are kept the excited wave amplitudes, $\mathbf{e}^{\pm}$, may be directly determined from Eq. (25) as

$$\begin{bmatrix} \mathbf{e}^+ \\ \mathbf{e}^- \end{bmatrix} = \begin{bmatrix} \mathbf{\Phi}_q^+ & -\mathbf{\Phi}_q^- \\ \mathbf{\Phi}_f^+ & -\mathbf{\Phi}_f^- \end{bmatrix}^{-1} \begin{bmatrix} \mathbf{0} \\ \mathbf{f}_{\text{ext}} \end{bmatrix}. \tag{26}$$

However, numerical problems are likely to occur for complicated structures because of ill-conditioning of the matrix to be inverted. To avoid these problems, only certain wave modes are kept.

A numerical implementation is here proposed which exploits the orthogonality of the left and right eigenvectors of the transfer matrix, i.e. Eq. (17). Premultiplying Eq. (25) by the left eigenvector matrix $\mathbf{\Psi}^{\pm}$ gives

$$\begin{bmatrix} \mathbf{\Psi}_f^+ & \mathbf{\Psi}_q^+ \\ \mathbf{\Psi}_f^- & \mathbf{\Psi}_q^- \end{bmatrix} \begin{bmatrix} \mathbf{\Phi}_q^+ & -\mathbf{\Phi}_q^- \\ \mathbf{\Phi}_f^+ & -\mathbf{\Phi}_f^- \end{bmatrix} \begin{bmatrix} \mathbf{e}^+ \\ \mathbf{e}^- \end{bmatrix} = \begin{bmatrix} \mathbf{\Psi}_f^+ & \mathbf{\Psi}_q^+ \\ \mathbf{\Psi}_f^- & \mathbf{\Psi}_q^- \end{bmatrix} \begin{bmatrix} \mathbf{0} \\ \mathbf{f}_{\text{ext}} \end{bmatrix}, \tag{27}$$

which leads to

$$\begin{bmatrix} \mathbf{\Psi}^+\mathbf{\Phi}^+ & \mathbf{0} \\ \mathbf{0} & -\mathbf{\Psi}^-\mathbf{\Phi}^- \end{bmatrix} \begin{bmatrix} \mathbf{e}^+ \\ \mathbf{e}^- \end{bmatrix} = \begin{bmatrix} \mathbf{\Psi}_q^+\mathbf{f}_{\text{ext}} \\ \mathbf{\Psi}_q^-\mathbf{f}_{\text{ext}} \end{bmatrix}. \tag{28}$$

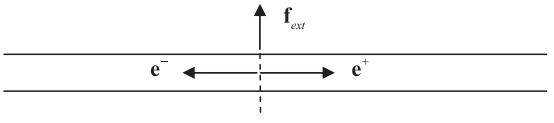

Fig. 5. Waves directly excited by local harmonic excitation applied at a point.

If the eigenvectors are normalised so that $d_i = 1$ in Eq. (17) then $\mathbf{\Psi}^{\pm}\mathbf{\Phi}^{\pm} = \mathbf{I}$. With these normalised eigenvectors, Eq. (28) becomes

$$\begin{aligned} \mathbf{e}^{+} &= \mathbf{\Psi}_q^{+}\mathbf{f}_{\text{ext}}, \\ \mathbf{e}^{-} &= -\mathbf{\Psi}_q^{-}\mathbf{f}_{\text{ext}}. \end{aligned} \tag{29}$$

Eq. (29) is always well-conditioned and the ill-conditioning in Eq. (26) can be removed.

3.2. Total wave amplitude: wave superposition

The displacement of the waveguide is in general expressed as (Eq. (19))

$$\mathbf{q} = \mathbf{\Phi}_q^{+}\mathbf{a}^{+} + \mathbf{\Phi}_q^{-}\mathbf{a}^{-} = \sum_{i=1}^{m}(\boldsymbol{\phi}_{q,i}^{+}a_i^{+} + \boldsymbol{\phi}_{q,i}^{-}a_i^{-}). \tag{30}$$

The wave amplitudes $a_i^{\pm}$ can be determined considering wave propagation, and subsequent reflection if the waveguide has a boundary. Consider a waveguide forming a circular shape as shown in Fig. 6. The wave amplitudes $\mathbf{a}^{+}$ and $\mathbf{g}^{-}$ travelling away from the excitation point are given by the sum of the directly excited waves $\mathbf{e}^{+}$ and $\mathbf{e}^{-}$ and the incident waves $\mathbf{a}^{-}$ and $\mathbf{g}^{+}$ by

$$\begin{aligned} \mathbf{a}^{+} &= \mathbf{e}^{+} + \mathbf{g}^{+}, \\ \mathbf{g}^{-} &= \mathbf{e}^{-} + \mathbf{a}^{-}. \end{aligned} \tag{31}$$

The incident waves, found by considering wave propagation around the circumference, are

$$\mathbf{g}^{+} = \boldsymbol{\tau}^{*}(2\pi)\mathbf{a}^{+}; \quad \mathbf{a}^{-} = \boldsymbol{\tau}^{*}(2\pi)\mathbf{g}^{-} \tag{32}$$

where

$$\boldsymbol{\tau}^{*}(\phi) = \text{diag}\{\exp(-\text{j}k_1^{*}\phi), \exp(-\text{j}k_2^{*}\phi), \ldots, \exp(-\text{j}k_n^{*}\phi)\} \tag{33}$$

is the wave propagation matrix, ϕ is an angle around the circumference of the circle,

$$k^{*} = kR \tag{34}$$

is the polar wavenumber and R is a radius. The case $k^{*} = n$, with n an integer, corresponds to the nth resonance in the circumferential. The wave amplitudes at the input point $\mathbf{a}^{\pm}$ can thus be expressed as

$$\begin{aligned} \mathbf{a}^{+} &= \{\mathbf{I} - \boldsymbol{\tau}^{*}(2\pi)\}^{-1}\mathbf{e}^{+}, \\ \mathbf{a}^{-} &= \{\mathbf{I} - \boldsymbol{\tau}^{*}(2\pi)\}^{-1}\mathbf{e}^{-} - \mathbf{e}^{-} \end{aligned} \tag{35}$$

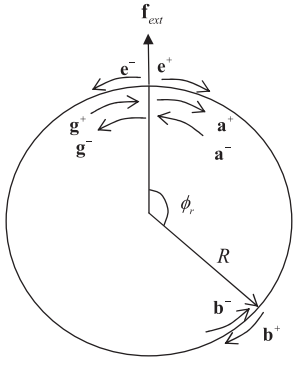

Fig. 6. Waves in a circular structure.

The wave amplitudes at some response point are

$$\mathbf{b}^{+} = \boldsymbol{\tau}^{*}(\phi_r)\mathbf{a}^{+},$$
$$\mathbf{b}^{-} = \boldsymbol{\tau}^{*}(2\pi - \phi_r)(\mathbf{a}^{-} + \mathbf{e}^{-}) \tag{36}$$

where ϕ_r is the angle between the excitation and the response point. The physical response is then found from Eq. (19).

4. WFE modelling of a tyre

A 'slick' tyre attached to an aluminium rim, as shown in Fig. 7, together with material data was provided by Bridgestone Corporation. A tyre can be regarded as a one-dimensional waveguide in the circumferential direction. In this section, a WFE model of the tyre is described. Frequency dependent material properties of rubber are considered.

4.1. Modelling of a short segment

A short segment of the tyre was modelled as shown in Fig. 8 using ANSYS 7.1. The coordinates and representative dimensions are shown in Fig. 9. The eight node solid element SOLID 46, which generates

Fig. 7. Tyre (195/65R15) with an aluminium rim.

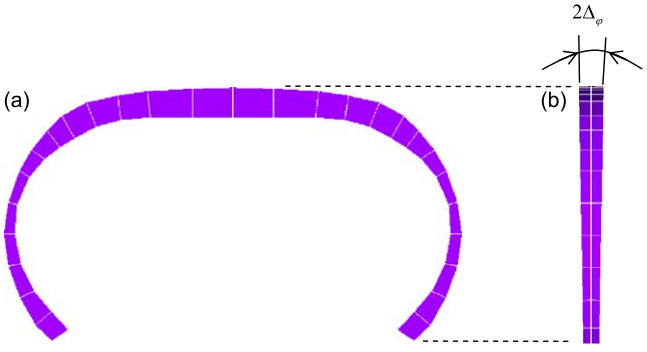

Fig. 8. Segment of the WFE tyre model: (a) tyre cross-section; (b) segment in the circumferential direction.

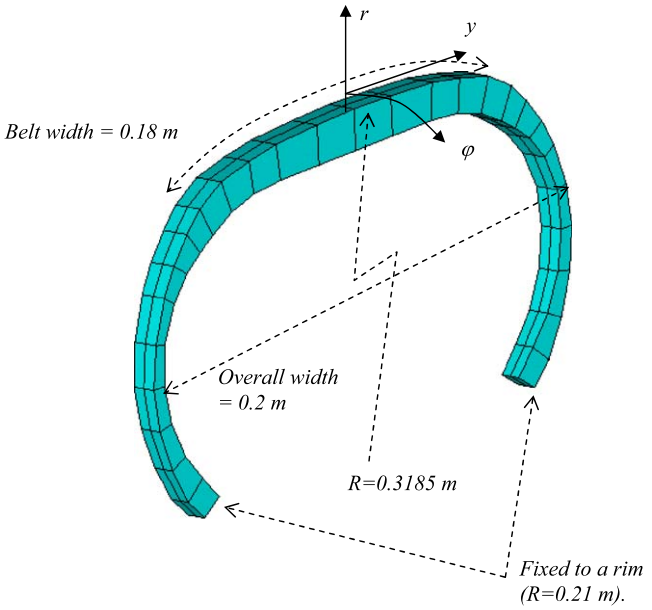

Fig. 9. Coordinates and a WFE model of the tyre segment.

equivalent anisotropic material properties for a layered structure, was used to represent the layered structure as shown in Fig. 1. The element has three translational dofs at each node. 28 elements were used to model the cross-section.

A segment of the tyre subtending an angle of $2\Delta_\varphi = 1.8^\circ$ was modelled. To represent the curvature of the tyre, adjacent segments of the tyre are connected together with their local coordinates being rotated through angles of $\pm\Delta_\varphi(0.9^\circ)$. This models the curved tyre as being composed of piecewise-plane elements. An internal pressure of 200 kPa was simulated by the application of surface loads on the elements [27,35]. Boundary conditions at the wheel rim were imposed by setting the dofs to zero. The number of dofs was 324 after the condensation of interior dofs.

4.2. Inclusion of frequency dependent material properties of rubber

Material properties of rubber depend on frequency [26]. To include the frequency dependent properties of rubber, the stiffness matrix was decomposed as

$$\mathbf{K}(f) = \mathbf{K}_{\text{fibre}} + \mathbf{K}_{\text{rubber}}(f) + \mathbf{K}_{\text{tension}} \tag{37}$$

where $f = \omega/2\pi$ is frequency in Hz. The stiffness matrices $\mathbf{K}_{\text{fibre}}$ and $\mathbf{K}_{\text{tension}}$ represent the frequency independent contributions of the fibres and the in-plane tension due to the internal pressure. The latter was derived from the difference between two stiffness matrices associated with FE models with and without the internal pressure. The stiffness matrix of the rubber elements is frequency dependent. If Poisson's ratio is assumed constant, the stiffness matrix is proportional to the Young's modulus E. The frequency dependent stiffness matrix $\mathbf{K}_{\text{rubber}}(f)$ at frequency f is then given by

$$\mathbf{K}_{\text{rubber}}(f) = \frac{E(f)}{E(f_0)}\mathbf{K}_{\text{rubber}}(f_0)\{1 + \mathrm{j}\eta(f)\} \tag{38}$$

where $\eta(f)$ is the frequency dependent loss factor and f_0 is a reference frequency at which the stiffness matrix $\mathbf{K}_{\text{rubber}}(f_0)$ is evaluated (neglecting damping). Eq. (38) allows one to include the frequency dependent stiffness and loss factor without remodelling the structure.

To determine $E(f)$ and $\eta(f)$ in Eq. (38), the rubbers were assumed to behave in the same manner as the American National Standards Institute (ANSI) standard polymer for which data is available in the literature

[36]. In the frequency range of interest ($0<f\leqslant 2$kHz, 30 °C), $E(f)$ and $\eta(f)$ may be approximated by [36]

$$\log(E(f)) = \alpha_E \cdot \log(f) + \beta_E, \tag{39}$$

$$\eta(f) = \alpha_\eta \cdot \log(f)^2 + \beta_\eta. \tag{40}$$

The coefficients were estimated from Ref. [36] to be $\alpha_E = 0.1$, $\alpha_\eta = 0.01$, $\beta_\eta = 0.1$ and β_E was determined from given material data for each rubber.

For the tyre model, the effect of the change in the stiffness of the rubber is relatively small in the frequency range analysed because the magnitudes of the elements of $\mathbf{K}_{\text{fibre}}$ (and $\mathbf{K}_{\text{tension}}$) are much larger than the changes in the elements of $\mathbf{K}_{\text{rubber}}(f)$. The Young's modulus of the rubber is typically of the order of $O(10^7)$ and changes in the Young's modulus are of the same order. On the other hand, the Young's modulus of the textile fibres is $O(10^9)$ and that of the steel fibres is $O(10^{11})$.

5. Free vibration

In this section the dispersion curves are presented including results for purely real, purely imaginary and complex wavenumbers. No damping is assumed for clarity. Complicated dispersion curves are presented. Phenomena such as curve veering and cut-on with a non-zero wavenumber are observed. Waves in which the

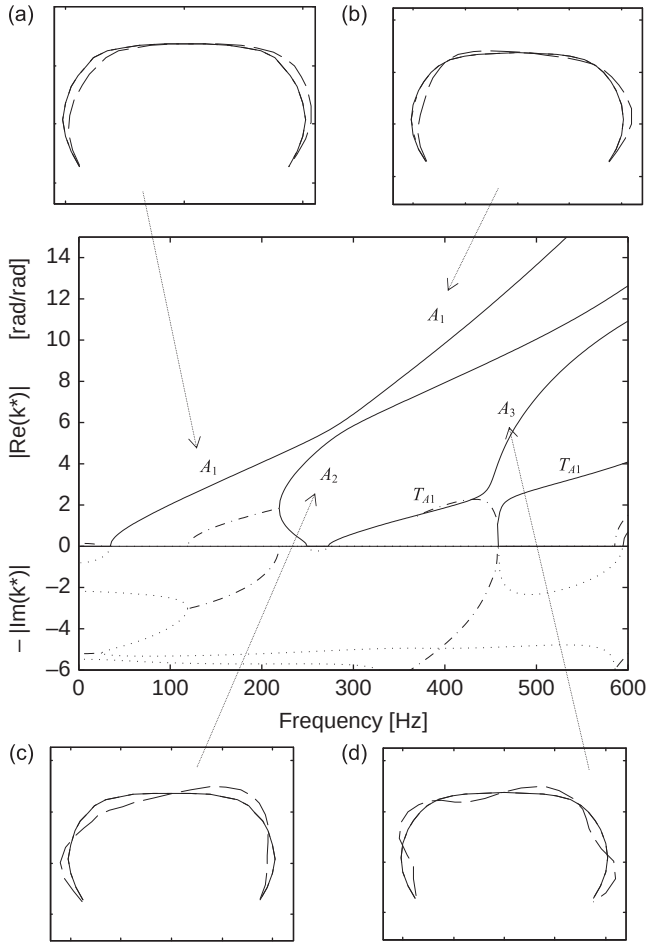

Fig. 10. Dispersion curves of the tyre for the asymmetric modes: — purely real; · · · purely imaginary; –·– complex conjugate wavenumbers. T_i denotes the shear wave mode. Small figure (a)–(d) illustrates the deformation associated with each wave mode: ___ original shape and - - - deformed shape.

group velocity and the phase velocity are of opposite signs are observed. Bifurcations from two different purely imaginary to complex conjugate wavenumbers and vice versa are illustrated. The group velocities are numerically determined from the power and energy relationship.

5.1. Dispersion curves

The dispersion curves are numerically determined from the WFE model of the tyre. For $\mathrm{Re}\{k\} \geqslant 0$, the dispersion curves below 600 Hz are shown in Fig. 10 for the asymmetric modes (A_i) and in Fig. 11 for the symmetric (S_i) modes. Only the wavenumbers which are associated with predominantly flexural or predominantly transverse shear motions in the cross-section of the tyre are plotted. The polar wavenumber (rad/rad) $k^* = kR(R = 0.3185)$ is shown. Natural frequencies occur when $k^* = 1, 2 \ldots$ for the k*th circumferential mode order and also at $k^* = 0$ for a breathing mode. Results for purely real, purely imaginary and complex (conjugate) wavenumbers are shown. Only wavenumbers for which $\mathrm{Im}(k)$ is small are shown for clarity. Wave modes in which the wave is characterised by predominantly transverse shear and/or longitudinal motion are denoted by T_{A_i} or T_{S_i}.

The asymmetric A_1 wave mode cuts-on first at about 35 Hz (Fig. 10). This mode comprises side-to-side motion of the tread as illustrated in Fig. 10(a). The A_1 wave mode and the symmetric S_1 wave mode (Fig. 11(a)) are bouncing modes where the tread mass is vibrating on the sidewall stiffness. The A_2 (Fig. 10(c)),

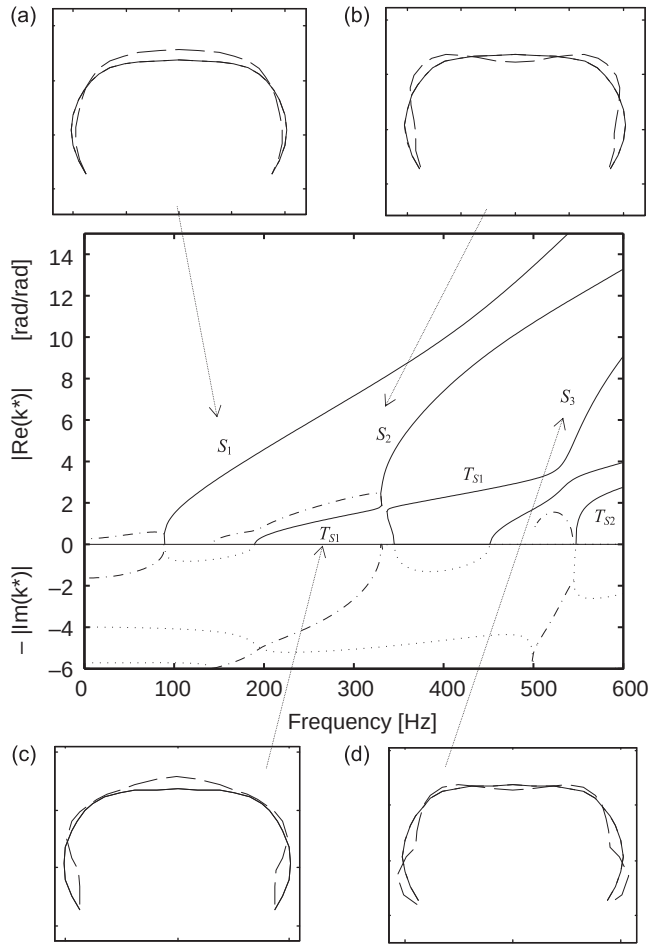

Fig. 11. Dispersion curves of the tyre for the symmetric modes: — purely real; · · · purely imaginary; –·– complex conjugate wavenumbers. T_i denotes the shear wave mode. Small figure (a)–(d) illustrates the deformation associated with each wave mode: ___ original shape and - - - deformed shape.

S_2 (Fig. 11(b)) and higher wave modes are cross-sectional modes where the cross-sectional deformation becomes more complex, with more nodes of the wave mode across the cross-section.

All wavenumbers at low frequencies are purely imaginary or part of a complex conjugate pair. Complex conjugate wavenumbers can bifurcate into two purely imaginary or purely real wavenumbers. In Fig. 10 a bifurcation from two different purely imaginary to complex conjugate wavenumbers is seen around 120 Hz. Below 120 Hz there are two purely imaginary wavenumbers associated with the A_2 and T_{A1} wave modes. At 120 Hz the wavenumbers become a complex conjugate pair in which the wave modes are associated with both the A_2 and T_{A1} motions. Another bifurcation from complex conjugate into two real wavenumbers can be seen at 220 Hz. At 220 Hz the imaginary parts of the complex conjugate wavenumbers become zero and waves start propagating with a non-zero purely real wavenumber. Above the cut-on frequency one wavenumber increases with frequency while the other decreases. For the frequency range where the wavenumber decreases with frequency, the wave is characterised by the phase and group velocities having opposite signs. The wave cuts-off at 250 Hz and the wavenumber becomes purely imaginary. The wavenumber becomes purely real again at 273 Hz and the wave starts propagating as the T_{A1} wave mode.

Around 280 Hz in Fig. 10, curve veering between the dispersion curves for the A_1 and A_2 wave modes is seen. When two wave modes are not orthogonal in the wave domain and their wavenumbers are nearly equal, dispersion curves do not cross each other and the wavenumbers rapidly change. Such a phenomenon is called curve veering, e.g. [37,38]. The shape of the wave mode changes around the frequency where the veering occurs. An example is shown in Figs. 10(a) and (b) for the A_1 mode.

The phenomena discussed above can be seen in Fig. 11 for the symmetric wave modes. In particular complicated cut-on phenomena are observed around 330 Hz where the S_2 wave mode cuts-on. The dispersion curves around the cut-off of the S_2 mode are shown in Fig. 12 for a narrow frequency range around the cut-off frequency. The non-zero cut-off of the S_2 mode occurs at around 326.8 Hz above which frequency there are two propagating waves. One wavenumber increases with frequency and the other decreases and becomes complex (conjugate) around 327.0 Hz where the S_2 and T_{S1} modes couple. The complex conjugate waves again become two propagating waves at around 332.8 Hz.

All the propagating wavenumbers associated with symmetric wave modes in the frequency range of interest, i.e. up to 2 kHz, are shown in Fig. 13. In total 8 wave modes propagate at 1 kHz and there are 4 S_i and 4 T_i wave modes. At 2 kHz 16 waves propagate (8 S_i and 8 T_i wave modes) in total. Veering between successive mode orders is clear.

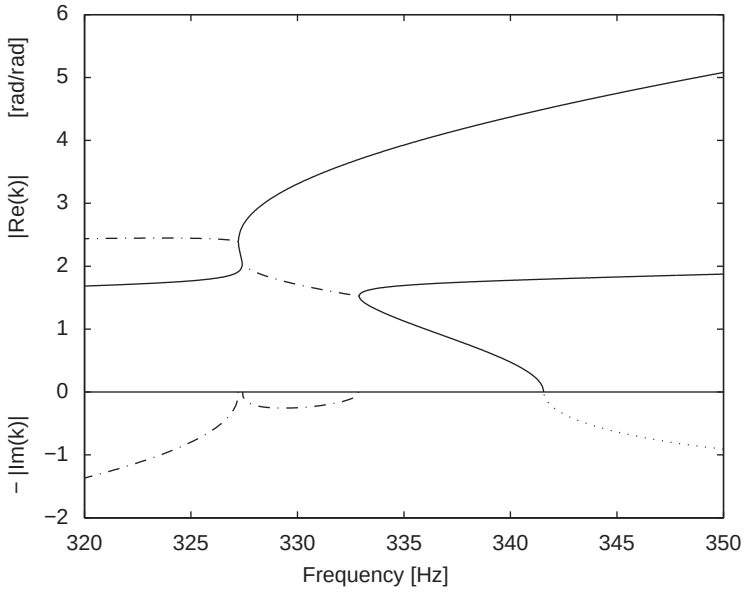

Fig. 12. Dispersion curves around the cut-on of the S_2 mode: — purely real; · · · purely imaginary; – · – complex conjugate wavenumbers.

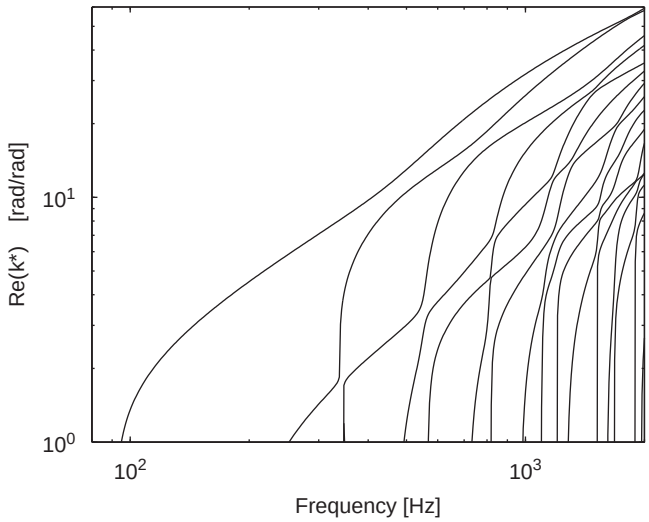

Fig. 13. Dispersion curves for propagating waves of the symmetric modes.

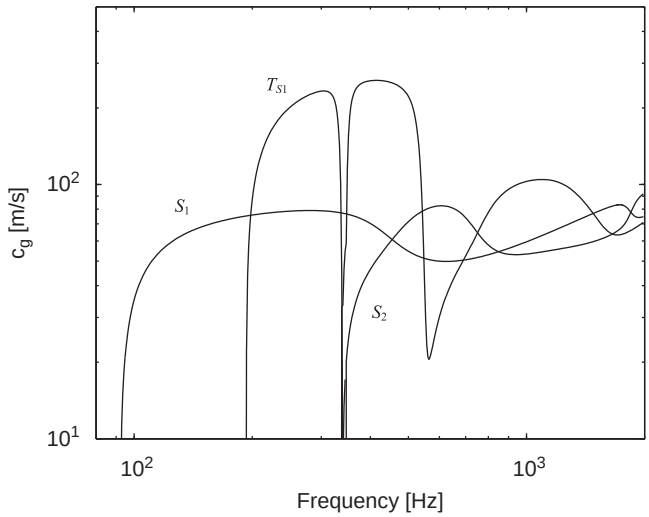

Fig. 14. Group velocities for the S_1, S_2, T_{s1} modes.

5.2. Group velocity

The group velocity can be calculated numerically using the power and energy relationship Eq. (22). The group velocities associated with the S_1, S_2, T_{S1} modes are shown in Fig. 14. The group velocity associated with predominantly flexural motion (S_1, S_2) is typically about 80 m/s (80π rad/s) and that for shear motion (T_{S1}) is about 240 m/s (240π rad/s). These values are similar to results in [16]. Fig. 15 focuses on the frequencies where the S_2 mode cuts-on. Three waves propagate in the frequency between 333 and 341 Hz and between 326.8 and 327.0 Hz. For both frequency ranges shown there is one wave propagating in the positive direction with a positive group velocity but a negative phase velocity.

6. Forced vibration

In this section the forced response of the tyre, calculated using the wave approach described in Section 3, is presented and compared with experimental data. Damping is included. In the experiments excitation was

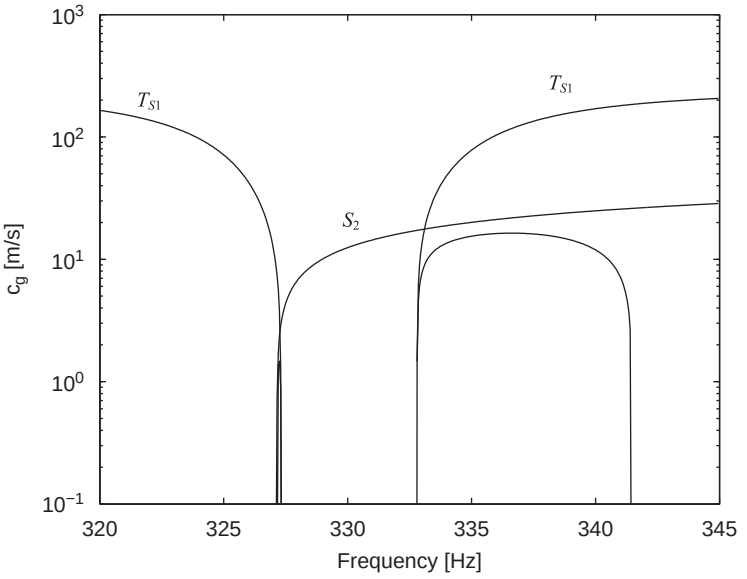

Fig. 15. Group velocities for the S_2, T_{s1} modes.

Fig. 16. Experimental setup.

applied to the centre of the tread of the tyre such that only the symmetric wave modes are strongly excited. The size of the region over which the excitation is applied affects the response, especially at high frequencies.

6.1. Experimental setup

The tyre attached to the rim was suspended using flexible rubber strings as shown in Fig. 16. The excitation was a random signal applied by a shaker attached to the tread centre through a relatively rigid metal disc of diameter $d = 23.5$ mm and 1 mm thickness as shown in Fig. 17. As the measured tyre was freely suspended, the dynamic response below 30 Hz is dominated by rigid body motions [27]. Also a resonance of the experimental rig occurs at around 2700 Hz [27] such that measured data is expected to be reliable between 30 and 2700 Hz. Measured signals were analysed using a Hanning window and averaged (at least 30 averages).

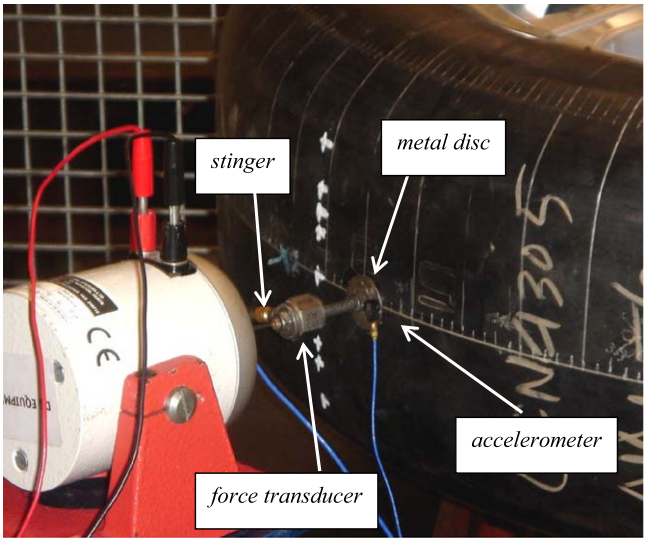

Fig. 17. Excitation arrangement.

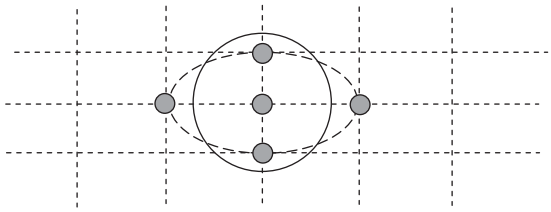

Fig. 18. Modelling the excited region: — experimental; – – numerical modelling: o nodes where excitations are applied; - - - the FE mesh.

The room temperature was about 30 °C throughout the measurement. Mass cancellation [39] was applied by post-processing the measured data to cancel the mass loading of the force transducer and the accelerometer.

Various limitations of the WFE model to predict the behaviour of the experiment must be acknowledged. The boundary conditions at the rim are assumed fixed, so that rigid body modes, whose effects are particularly noticeable below 30 Hz, are not modelled and nor are modes of the rim. The presence of air in the tyre, apart from its effect in inducing tension in the tyre, is also not modelled. There are consequently acoustic cavity resonances whose effects are not modelled. These are, however, only important over very limited frequency ranges [19]. Including these is the subject of future work. Finally no attempt has been made to update the model parameters: manufacturer's data and the ANSI polymer model of Eqs. (39) and (40) were used. All these limit the expected accuracy.

6.2. *Forced response of a tyre with finite area excitation*

The forced response is calculated using the wave approach. A frequency dependent loss factor $\eta(f)$ for the rubber was included in Eq. (38). The waves with small values of $|\mathrm{Im}(k^*)|$ were retained to calculate the forced response. The resulting number of kept positive- and negative going wave pairs in the frequency range analysed was about 70. In the experiment excitation was applied through a relatively rigid disc. In the analysis this was simulated by point forces applied at a number of nodes as shown in Fig. 18. The excitation applied in the experiment was modelled as being distributed over an oval shape such that the areas excited are the same. The weighted average responses from 5 different excitation points corresponding to these nodes were found. The relative weights chosen for each node were in proportion to the area excited.

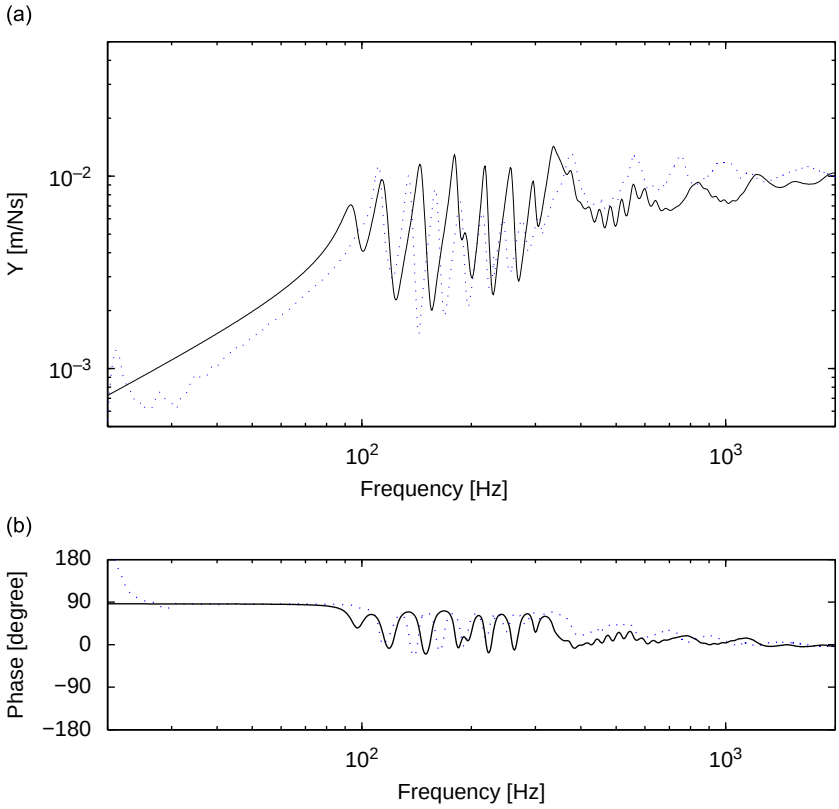

Fig. 19. (a) Magnitude and (b) phase of the input mobility at the tread centre of the tyre: — the WFE result; · · · experiment.

The predicted and measured forced responses of the tyre are shown in Fig. 19. Reasonable agreement between the predicted results and the measured data can be seen. Note that no attempt was made to update the data provided by the manufacturer. Doing this would of course improve the agreement.

The response of the tyre can be divided into three regions. Below the first resonance at around 90 Hz, where the S_1 mode cuts-on, the sidewall stiffness is dominant and the response is stiffness controlled. The effects of rigid body modes are also most noticeable in this frequency range. Above the first resonance, and up to 300 Hz or so, there are several resonance peaks associated with vibrational modes of the tyre around the circumference, with the deformation across the tread and sidewall being in the S_1 mode. Here the response is similar to that of a beam on an elastic foundation. Above 350 Hz, where the S_2 mode cuts-on, the response becomes more or less constant. Because of the level of damping individual resonances overlap and distinct resonance peaks cannot be clearly identified. At high frequencies the response tends to that of a plate with finite shear stiffness, or that of an elastic half space with excitation applied over a finite area. This is discussed further in the next subsection.

The predicted frequency of the first resonance is smaller than the measured result, but the frequency difference between successive peaks is larger. This implies that the stiffness across the tread and sidewall is smaller than that of the real tyre but that in the circumferential direction is larger.

6.3. *Effect of the size of the excited area*

The structural response is particularly sensitive to the spatial distribution of the excitation at high frequencies where the wavelengths become small. For example, consider an excitation of uniform force f_0 per unit length, applied along a line of length $2r$. The force injected into a wave mode with wavenumber k takes

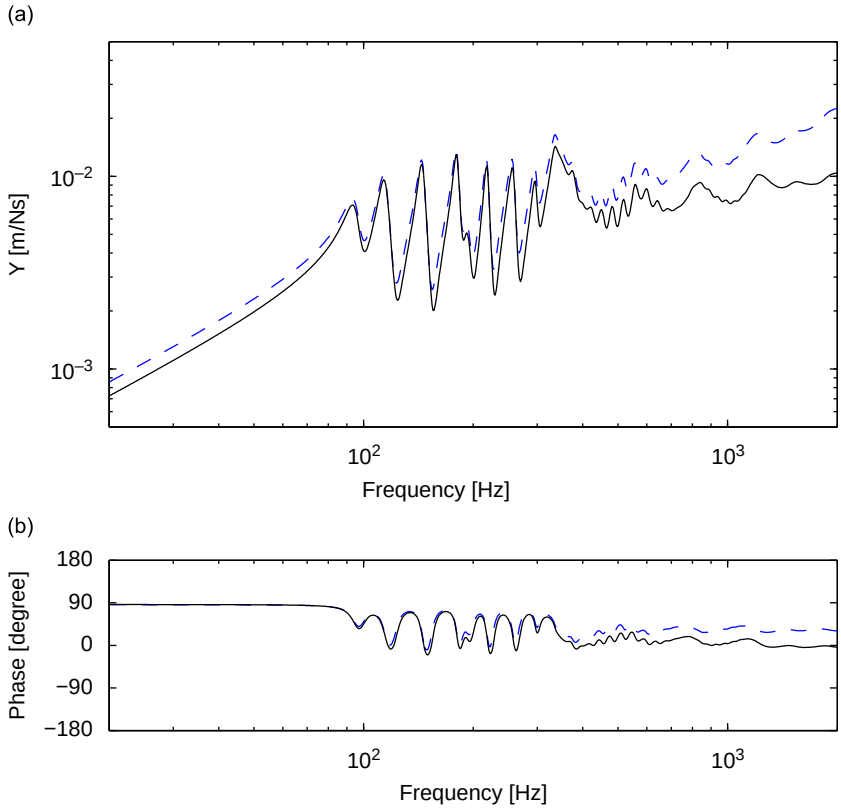

Fig. 20. (a) Magnitude and (b) phase of the predicted input mobility of the tyre for — the finite area excitation; – – a point excitation.

the form

$$f(k)\sim\frac{f_0}{2\pi}\int_{-r}^{r}\exp(\mathrm{j}kr)\,\mathrm{d}r=\frac{f_0 r}{\pi}\frac{\sin(kr)}{kr}. \tag{41}$$

For $kr\ll 1$, Eq. (41) gives $f(k)\approx f_0 r/\pi$ and the value is independent of k. But for $kr=O(1)$ or larger, the effective force on the wave mode decreases and the wave is not excited as strongly.

In addition, if the thickness of the structure, h, is not small enough compared to the radius of excitation, typically when $h/r\geqslant 5$, the response of the structure approaches that of an elastic half space so that the shear stiffness and local stiffness become more important [40].

To illustrate the effect of the spatial distribution of the excitation, the responses of the tyre for both the finite area excitation and point excitation are shown in Fig. 20. At low and moderate frequencies the responses are almost the same but their asymptotes at high frequencies differ. The shear deformation becomes more important for the point force excitation and the response becomes reactive. These numerical results show that the dynamic behaviour of a tyre at high frequencies can be strongly affected by the distribution of the excitation and also that an assumption of a 'thin' structure can break down.

7. Conclusions

Free and forced vibrations of a tyre were predicted using a WFE method. A short segment of the tyre was modelled using a commercial software package (ANSYS). The dynamic stiffness matrix of the segment was post-processed to extract free wave propagation characteristics. Since only a short segment needs to be modelled, the resulting number of dofs (324 in the example shown) is small and the calculation cost is small. The eigenvalue problem is solved at each selected frequency. Frequency dependent material properties of rubber can therefore be included straightforwardly.

Free wave propagation was predicted and complicated dispersion phenomena were observed. Curve veering between dispersion curves was observed and rapid changes of the wavenumber were shown. The non-zero cut-on phenomena was also seen for waves for which the predominantly flexural and longitudinal and/or shear waves couple. Associated with the non-zero cut-on phenomena, the existence of a pair of propagating waves for which the signs of the phase and group velocities are opposite were observed.

The forced response was calculated using the wave approach. The amplitudes of directly excited waves were found first using a well-conditioned formulation and a reduced basis, i.e. by retaining only the most important wave modes. The total wave amplitudes were found by superposition, considering wave propagation around the tyre in the circumferential direction. The predicted results were compared with experiment results and good agreement was seen. At high frequencies the response approaches that of a plate with finite shear stiffness or that of an elastic half space. The size of the region over which excitation is applied was discussed. This affects the response and was seen to be particularly important at high frequencies. In summary, the WFE method allows predictions to be made of the vibrational response of a tyre to many kHz, at low computational cost and including details of the construction of the tyre.

References

[1] U. Sandberg, J.A. Ejsmont, Tyre/Road Noise Reference Book. Informex, 2002.
[2] J.R. Cho, K.W. Kim, H.S. Jeong, Numerical investigation of tire standing wave using 3-D patterned tire model, *Journal of Sound and Vibration* 305 (2007) 795–807.
[3] M. Brinkmeier, U. Nackenhorst, S. Petersen, O. vonEstorff, A finite element approach for the simulation of tire rolling noise, *Journal of Sound and Vibration* 309 (2008) 20–39.
[4] K.F. Graff, *Wave Motion in Elastic Solids*, Dover, New York, 1975.
[5] F. Böhm, Mechanik des Gürtelreifens, *Ingenieru Archiv* 35 (1966) 82–101.
[6] R.J. Pinnington, A wave model of a circular tyre. Part 1: belt modelling, *Journal of Sound and Vibration* 290 (2006) 101–132.
[7] W. Kropp, Structure-borne sound on a smooth tyre, *Applied Acoustics* 26 (1989) 181–192.
[8] K. Larsson, W. Kropp, A high-frequency three-dimensional tyre model based on two coupled elastic layers, *Journal of Sound and Vibration* 253 (4) (2002) 889–908.
[9] F. Wullens, W. Kropp, A three-dimensional contact model for tyre/road interaction in rolling conditions, *Acta Acustica United with Acustica* 90 (2004) 702–711.
[10] W. Kropp, K. Larsson, F. Wullens, P. Andersson, Tyre/road noise generation—modelling and understanding, *Proceedings of the Institute of Acoustics* 26 (2) (2004) 1–12.
[11] P. Andersson, K. Larsson, F. Wullens, W. Kropp, High frequency dynamic behaviour of smooth and patterned passenger cars, *Acta Acustica United with Acustica* 90 (2004) 445–456.
[12] R.J. Pinnington, A.R. Briscoe, A wave model for a pneumatic tyre belt, *Journal of Sound and Vibration* 253 (5) (2002) 941–959.
[13] R.J. Pinnington, A wave model of a circular tyre. Part 2: side-wall and force transmission modelling, *Journal of Sound and Vibration* 290 (2006) 133–168.
[14] J.M. Muggleton, B.R. Mace, M.J. Brennan, Vibrational response prediction of a pneumatic tyre using an orthotropic two-plate wave model, *Journal of Sound and Vibration* 264 (2003) 929–950.
[15] J.S. Bolton, H.J. Song, Y.K. Kim, Y.J. Kang, The wave number decomposition approach to the analysis of tire vibration, *Proceedings of NOISE-CON* 98 (1998) 97–102.
[16] Y.J. Kim, J.S. Bolton, Modeling of tire treadband vibration, in: *Proceedings of Inter-Noise 2001*, Hague, Netherlands, 2001, pp. 2605–2610.
[17] S. Finnveden, Evaluation of modal density and group velocity by a finite element method, *Journal of Sound and Vibration* 273 (2004) 51–75.
[18] P.J. Shorter, Wave propagation and damping in linear viscoelastic laminates, *Journal of Acoustical Society of America* 115 (5) (2004) 1917–1925.
[19] C.M. Nilsson, Waveguide finite elements applied on a car tyre. Doctoral Thesis, Department of Aeronautical and Vehicle Technology, Royal Institute of Technology, Sweden, 2004.
[20] J.F. Doyle, *Wave Propagation in Structures*, second ed., Springer, Berlin, 1997.
[21] B.R. Mace, D. Duhamel, M.J. Brennan, L. Hinke, Finite element prediction of wave motion in structural waveguides, *Journal of the Acoustical Society of America* 117 (5) (2005) 2835–2843.
[22] D. Duhamel, B.R. Mace, M.J. Brennan, Finite element analysis of the vibrations of waveguides and periodic structures, *Journal of Sound and Vibration* 294 (2006) 205–220.
[23] J.M. Mencik, M.N. Ichchou, Wave finite elements in guided elastodynamics with internal fluid, *International Journal of Solids and Structures* 44 (2007) 2148–2167.
[24] L. Houillon, M.N. Ichchou, L. Jezequel, Wave motion in thin-walled structures, *Journal of Sound and Vibration* 281 (2005) 483–507.
[25] D.J. Thompson, Wheel-rail noise generation, part 3: rail vibration, *Journal of Sound and Vibration* 161 (3) (1993) 421–446.

[26] A.D. Nashif, D.I.G. Jones, J.P. Henderson, *Vibration Damping*, Wiley, New York, 1985.
[27] Y. Waki, On the application of finite element analysis to wave motion in one-dimensional waveguides. Ph.D. Thesis, ISVR, University of Southampton, 2007.
[28] M.I. Friswell, J.E. Mottershead, *Finite Element Model Updating in Structural Dynamics*, Kluwer Academic Publishers, Dordrecht, 1995.
[29] L. Brillouin, *Wave Propagation in Periodic Structures*, second ed, Dover, New York, 1953 (Chapter 2).
[30] W.X. Zhong, F.W. Williams, On the direct solution of wave propagation for repetitive structures, *Journal of Sound and Vibration* 181 (3) (1995) 485–501.
[31] D. Duhamel, B.R. Mace, M.J. Brennan, Finite element analysis of the vibrations of waveguides and periodic structures, ISVR Technical Memorandum no: 922, 2003.
[32] Y. Waki, B.R. Mace, M.J. Brennan, Waveguide finite element modelling: numerical issues and application to simple waveguides, *Proceedings of ISMA2006*, Leuven, 2006, pp. 2435–2449.
[33] L. Cremer, M. Heckl, B.A.T. Petersson, *Structure-Borne Sound*, third ed., Springer, Berlin, 2005 (Chapter 3, p. 60).
[34] N.R. Harland, B.R. Mace, P.W. Jones, Wave propagation, reflection and transmission in tunable fluid-filled beams, *Journal of Sound and Vibration* 241 (5) (2001) 735–754.
[35] ANSYS Inc. Corporate 2003 ANSYS 7.1 Manual Documentation.
[36] W.M. Madigosky, G.F. Lee, J.M. Niemiec, A method for modeling polymer viscoelastic data and the temperature shift function, *Journal of the Acoustical Society of America* 119 (6) (2006) 3760–3765.
[37] J.R. Kutter, V.G. Sigillito, On curve veering, *Journal of Sound and Vibration* 75 (4) (1981) 585–588.
[38] P.T. Chen, J.H. Ginsberg, Modal properties and eigenvalue veering phenomena in the axisymmetric vibration of spheroidal shells, *Journal of the Acoustical Society of America* 92 (3) (1992) 1499–1508.
[39] D.J. Ewins, *Modal Testing*, second ed., Research Studies Press, UK, 2000 (Chapter 3, p. 257).
[40] B.A.T. Petersson, M. Heckl, Concentrated excitation of structures, *Journal of Sound and Vibration* 196 (3) (1996) 295–321.